Chinese Chemical Letters 34 (2023) 107311

Contents lists available at ScienceDirect

Chinese Chemical Letters

journal homepage: www.elsevier.com/locate/cclet

Post-modification of metal-organic framework for improved CO_2 photoreduction efficiency

An-An Zhang[a,b,1], Rui Wang[a,b,1], Hai-Bo Huang[b], Tian-Fu Liu[b,c], Rong Cao[a,b,c,*]

[a] Department of Chemistry, School of Chemistry and Materials Science, University of Science and Technology of China, Hefei 230026, China
[b] State Key Laboratory of Structural Chemistry, Fujian Institute of Research on the Structure of Matter, Chinese Academy of Sciences, Fuzhou 350002, China
[c] Fujian Science and Technology Innovation Laboratory for Optoelectronic Information of China, Fuzhou 350002, China

ARTICLE INFO

Article history:
Received 5 January 2022
Revised 30 January 2022
Accepted 10 March 2022
Available online 13 March 2022

Keywords:
Metal-organic framework
Post-modification
Hydroxyl group
Ion exchange
CO_2 photoreduction

ABSTRACT

Utilizing metal-organic frameworks (MOFs) to design photocatalysts for CO_2 reduction catalysts is an excellent idea but currently restricted by the relatively low activity. Enhancing CO_2 affinity and tuning the oxidation state of metal clusters in MOFs might be a solution to improve the catalytic performance. Herein, the Cl-bridge atoms in the metal clusters of a cobalt MOF were easily exchanged with OH^-, which simultaneously oxidized a portion of Co(II) to Co(III) and resulted in a much enhanced photocatalytic activity for CO_2 reduction. In contrast, the original framework does not exhibit such superior activity. Comprehensive characterizations on their physicochemical properties revealed that the introduction of hydroxyl group not only greatly increases the CO_2 affinity but also alters the oxidation state of metal clusters, resulting in significantly improved photocatalytic activities for CO_2 reduction. This work provides important insight into the design of efficient photocatalysts.

Visible-light-photocatalytic reduction of CO_2 to valuable chemicals mimicking natural photosynthesis process is an effective way to mitigate the growing global energy crisis [1–6]. Metal-organic frameworks (MOFs), a type of porous crystalline material assembled by organic linkers and metal/metal cluster nodes through coordination bonds, have captured widespread interest in photocatalysis fields [7–9]. The metal nodes can act as catalytic active sites, and the porous structure shows high affinity toward the gaseous substrate. Therefore, MOFs present as ideal candidates to accumulate and then reduce CO_2 to CO and CH_4 by using the photogenerated electrons deriving from light excitation. However, the relatively low catalytic activity of MOFs has been a stumbling block for their potential applications. Therefore, improving the photocatalytic efficiency for CO_2 reduction is a long-lasting challenge for researchers in this field.

Post-modification syntheses have been proven as an effective strategy to tune MOF structures for improved catalytic performance [10–17]. Recently, a study reported that the divalent cobalt in an alkaline-stable MOF can be oxidized to trivalent cobalt through introducing OH^- into backbones *via* post-modification [18]. It has been established that the transition metal Co(III) is very active for many catalytic reactions [19]. Additionally, the hydroxyl group has a high affinity toward CO_2 [20]. Inspired by these findings, we speculated that integrating OH^- and highly-active Co(III) into a MOF structure may enhance the CO_2 photoreduction activity.

Herein, we report the successful post-modification of a cobalt MOF from Cl^- bridge to OH^- bridge by simple ion exchange. The influence of Cl^-/OH^- on the CO_2 photocatalytic activity and selectivity was systemically investigated, and the underlying mechanism was revealed by X-ray photoelectron spectroscopy (XPS), cyclic voltammetry (CV), and other characterizations. These experimental results demonstrate that the introduction of hydroxyl groups not only greatly increases the CO_2 affinity but also alters the oxidation state of metal clusters, resulting in significantly optimized catalytic kinetics and improved photocatalytic activities. The efforts and discoveries described here are expected to provide some insight into the design of effective photocatalysts.The MOF $[Co_2(\mu\text{-}Cl)_2(bbta)]$ (H_2bbta = 1*H*,5*H*-benzo-(1,2-*d*:4,5-*d*′)bistriazole, denoted as Co-Cl) was obtained according to the previous report [18]. In brief, H_2bbta and $CoCl_2{\cdot}6H_2O$ were ultrasonically dissolved in a mixture of *N*,*N*-dimethylformamide (DMF) and methanol (MeOH), which was heated at 70 °C for 72 h to yield pink needle microcrystals of Co-Cl. And Co-Cl possesses a three-dimensional (3D) coordination framework with a honeycomb-like structure. Each Co ion is coordinated

* Corresponding author at: Department of Chemistry, School of Chemistry and Materials Science, University of Science and Technology of China, Hefei 230026, China.
E-mail address: rcao@fjirsm.ac.cn (R. Cao).
[1] These authors contributed equally to this work.

https://doi.org/10.1016/j.cclet.2022.03.034
1001-8417/

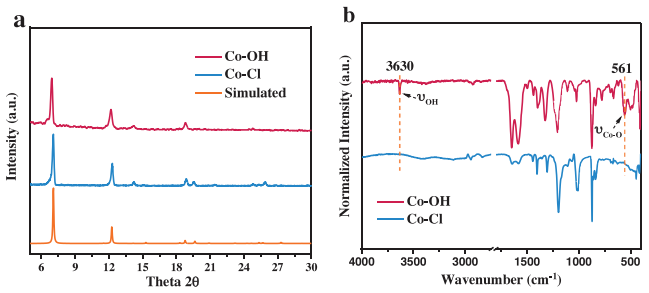

Fig. 1. (a) PXRD patterns of Co-Cl, Co-OH and simulated curve from single crystal X-ray data. (b) IR spectra of Co-Cl and Co-OH.

by three nitrogen atoms from three $bbta^{2-}$ ligands, two μ-Cl anions, and each $bbta^{2-}$ ligand coordinates to six Co ions. The Co ions are bridged by the μ_3-triazolate ring and μ-Cl to form a helical chain, which are connected by the phenyl backbone of $bbta^{2-}$ to generate a pillared-rod structure with large 1D channels parallel to the helical chains. The replacement of bridging Cl^- with OH^- groups can be achieved by immersing Co-Cl in 1.0 mol/L KOH solution for 14 h at room temperature (denoted Co-OH). Powder X-ray diffraction (PXRD) pattern revealed that Co-OH maintained the pure and highly crystalline phase after the treatment (Fig. 1a). The stretching vibrations of OH^- at 3630 cm^{-1} and Co-O at 561 cm^{-1} were observed in infrared spectroscopy (IR) spectra (Fig. 1b), suggesting the successful introduction of hydroxo-bridge cobalt clusters in Co-OH. Moreover, X-ray photoelectron spectroscopy (XPS) analyses revealed that the Cl characteristic peak disappeared in the spectrum for Co-OH (Fig. S1 in Supporting information), indicating Cl^- was completely substituted by OH^-. Meanwhile, the morphologies of the as-prepared Co-OH retained after soaking in KOH as revealed by scanning electron microscopy (SEM), indicating its desired stability for the subsequent catalytic reaction (Figs. S2a and b in Supporting information). Moreover, the corresponding elemental mappings of O and Cl illustrated the absence of Cl in Co-Cl, which matches well with the results obtained from XPS studies. The contact-angle tests showed that Co-OH exhibited a smaller contact angle (32.1°) than Co-Cl (36.3°) did (Figs. S2c and d in Supporting information), which indicates that the hydrophilicity of material does not greatly change with replacing Cl^- by OH^-. The high hydrophilicity nature would be conducive to the water activation in the CO_2 reduction process [3]. The broad and strong light absorption at 400–700 nm for both Co-OH and Co-Cl ensure the full use of visible-light irradiation for photocatalysis (Fig. 2a). The bandgaps of Co-OH and Co-Cl were estimated to be 2.50 eV and 2.80 eV, respectively, from the Kubelka-Munk plots (Fig. 2b), indicating that OH^- modification barely impact on the energy gaps. Mott-Schottky measurements at 500, 1000, and 1500 Hz were used to investigate the semiconductor character and energy alignment of Co-OH and Co-Cl (Figs. 2c and d). The positive slope of the obtained C^{-2} value indicates the n-type semiconductor feature of these materials.

The conduction band minimum (CBM) was evaluated to be −1.83 V for Co-Cl, −1.14 V for Co-OH *vs.* Ag/AgCl electrodes (−1.63 V and −0.94 V *vs.* NHE, pH 7), which is more negative than the redox potentials of CO_2/CO (−0.51 V *vs.* NHE, pH 7) and CO_2/CH_4 (−0.24 V *vs.* NHE, pH 7). Based on the bandgap information obtained from the UV–vis spectrum, the valence band maximum (VBM) was estimated to be around 1.56 V for Co-OH and 1.17 V for Co-Cl (*vs.* NHE, pH 7). The replacement of Cl^- with OH^- resulted in a considerable change on the CBM position of the MOF, which might be attributed to the change on the valence state of Co centers. Although Co-OH has low N_2 uptakes than Co-Cl (Fig. 2e), there exists a noticeable hysteresis loop between adsorption and desorption branches, indicating a stronger N_2 affinity of Co-OH frameworks. The stronger N_2 affinities of Co-OH may be ascribed to the defects, which resulted in a slightly larger pore size distribution for Co-OH than for Co-Cl (Fig. S4 in Supporting information). CO_2 adsorption uptake of Co-OH is unexpectedly higher than that of Co-Cl, in contrast to nitrogen adsorption. According to Fig. 2f, Co-OH has considerably improved CO_2 binding affinities, as evidenced by the steep slopes at low pressures, the higher uptakes throughout the entire pressure range, and the hysteresis loops in isotherm. We can expect that this high CO_2 affinity would considerably improve the CO_2 photoreduction efficiency.

All the photocatalytic reactions of CO_2 and H_2O were conducted under visible-light illumination ($\lambda > 400$ nm) without the presence of hole scavengers. As indicated in Figs. 3a and b, the CH_4 generation rate was 0.53 μmol g^{-1} h^{-1} and the CO generation rate was 2.0 μmol g^{-1} h^{-1} for Co-Cl. In contrast, Co-OH showed a much increased CH_4 evolution rate as high as 9.8 μmol g^{-1} h^{-1}, although the CO generation rate is almost the same. To verify the origin of CH_4, N_2 instead of CO_2 was introduced into the reaction system as a reactant under similar conditions. In this case, only a trace amount (13 μmol/g) of CH_4 was obtained after 5 h. The maintained high crystallinity and the negligible decrease in the CH_4 and CO generation rate in four successive runs confirm the durability of Co-OH (Fig. 3d and Fig. S5 in Supporting information). H_2O_2 was confirmed as the oxidation product by the iodometric method [21–23]. The iodide ion (I^-) reacts with H_2O_2 and form triiodide ion (I_3^-) strongly absorbing at 352 nm (Fig. 3c) (more information can be seen in Supporting information). This unexpected increase in activity and selective illustrates the capability of this strategy for photocatalyst design, inspiring us to further look into the mechanism.

To better understand the charge transfer behavior of these samples, electrochemical impedance spectroscopy (EIS) studies were performed. Compared with Co-Cl, the semicircle radius of Co-OH curve dropped dramatically, showing a lower resistance (Fig. 4a). As a consequence, Co-OH has an improved conductivity and charge-carrier transfer efficiency, which is consistent with the photocatalytic activity trends. Meanwhile, Co-OH showed a lower fluorescence intensity than Co-Cl did, implying a greatly suppressed radiative electron-hole recombination in Co-OH (Fig. 4b). XPS spectra were acquired in order to comprehensively investigate the cause of the improved photocatalytic activity. The O 1s XPS spectra of Co-Cl shown in Fig. S6 (Supporting information) could be divided into two peaks centered at 531.7 and 533.3 eV, which may be attributed to adsorbed oxygen and surface hydroxyl groups, respectively [24,25].

While the peaks of Co-OH at 531.0 and 533.1 eV can be attributed to the lattice oxygen (Co-O) and surface hydroxyl groups, respectively, confirming the successful substitution of Cl^- with OH^- [24]. On the other hand, the Co 2P peaks could be fitted into two peaks at 782.8 and 780.8 eV in Co-Cl (781.5 and 780.5 eV in Co-OH), which can be assigned to Co(III) and Co(II) (Fig. 4c). This is consistent with the prediction that the Co(II) inside Co-OH bound to a terminal H_2O/OH^- ligand and was further oxidized to Co(III)-OH species [18]. However, the Co(III)/Co(II) ratio in Co-OH is three times higher than that in Co-Cl, implying that the majority of Co(II) of Co-OH was converted to Co(III) (Table S1 in Supporting information). In addition, the Co $2p_{1/2}$–$2p_{3/2}$ spin−orbit level energy spacing is 16 eV for Co-Cl and 15 eV for Co-OH, this is also an indicative of +3 oxidation state for the majority of the Co species in Co-OH [26,27]. Other evidence came from the lower binding energy of Co(III) (blue part) in Co-OH than that in Co-Cl, indicating that Co-OH has a higher electron cloud density. Based on the XPS data, we can conclude that there exists a large amount of Co(III) spices in Co-OH after post-modification, which is assumed to an important reason for the increased activity [19]. Cyclic voltamme-

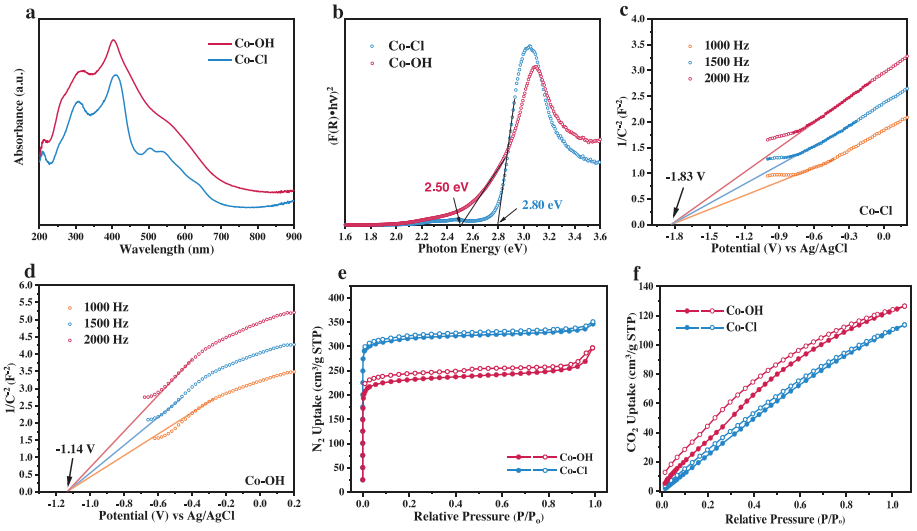

Fig. 2. (a) Ultraviolet-visible (UV–vis) diffuse-reflectance spectrum (DRS) of Co-Cl and Co-OH. (b) DRS of Co-Cl and Co-OH *via* K-M transformation. Mott−Schottky plot of (c) Co-Cl and (d) Co-OH electrode. (e) N_2 isotherms at 77 K and (f) CO_2 isotherms at 298 K for Co-Cl and Co-OH.

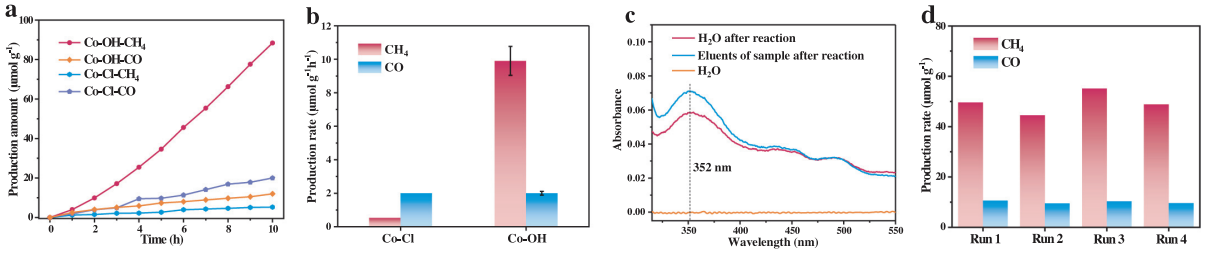

Fig. 3. (a) Time-dependent CH_4 and CO evolution curves. (b) CH_4 and CO evolution rate histograms. error bars mean ± standard deviations calculated from three independent measurements. (c) Hydrogen peroxide concentrations were determined using the iodometric method. The iodide ion (I^-) reacts with H_2O_2 to form the triiodide ion that absorbs strongly at 352 nm. The eluents of sample after reaction: Take 1 mL of water to rinse and filter the sample after the reaction. (d) The CH_4 and production rate histograms in the cycling experiments over Co-OH.

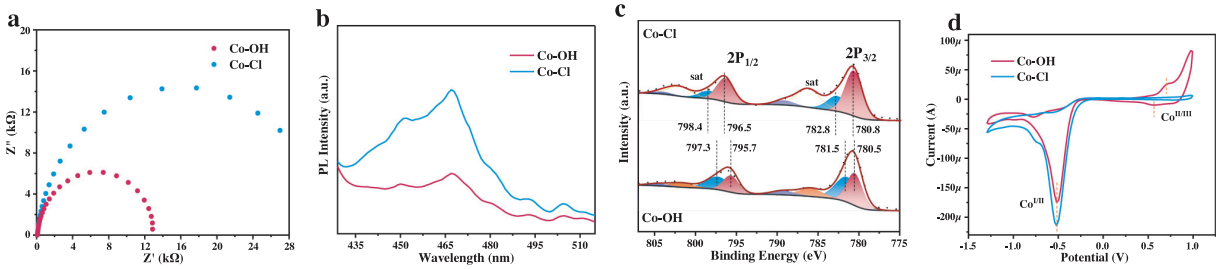

Fig. 4. (a) EIS of the Co-Cl and Co-OH. (b) Solid-state PL spectra of Co-Cl and Co-OH excited at λ = 418 nm. (c) XPS in Co 2p for Co-Cl and Co-OH. (d) The cyclic voltammetry curves of Co-Cl and Co-OH.

try (CV) can provide more information about the redox behavior of material and the possible catalytic process during reaction. As revealed in Fig. 4d, both Co-Cl and Co-OH show irreversible Co^{II}/Co^{I} peaks at $E = -0.51$ V (*vs.* Ag/AgCl), while Co-OH shows an extra reversible reductive process peak at $E_{1/2} = 0.64$ V which can be assigned to the redox of Co^{II}/Co^{III} [27–30]. Moreover, the peak current for Co^{II}/Co^{I} peak in Co-OH is lower than that of Co-Cl, implying a decrease of Co(II) component in Co-OH. The newly appeared Co^{II}/Co^{III} redox peak and the decreased Co(II) content further confirm the transform from Co(II) to Co(III).

In this work, the bridging Cl^- ions in the cobalt clusters of a Co-MOF were successfully replaced by OH^- ions *via* post-modification, resulting in a highly efficient and reusable visible-light photocatalyst for CO_2 reduction. The mechanistic analyses demonstrated that, compared with Cl^-, the introduction of OH^- causes a higher CO_2 affinity and partial oxidation of the cobalt nodes from Co(II) to Co(III), significantly boosting the with photocatalytic activity of materials. This work might shed light on the fabrication of highly active and stable MOF-based photocatalysts.

Declaration of competing interest

The authors declare no competing financial interest.

Acknowledgments

This work was financially supported by the National Key Research and Development Program of China (No. 2018YFA0208600), the National Natural Science Foundation of China (No. 22033008), Fujian Science & Technology Innovation Laboratory for Optoelectronic Information of China (No. 2021ZZ103).

Supplementary materials

Supplementary material associated with this article can be found, in the online version, at doi:10.1016/j.cclet.2022.03.034.

References

[1] R. Li, W. Zhang, K. Zhou, Adv. Mater. 30 (2018) 1705512.
[2] A. Dhakshinamoorthy, A.M. Asiri, H. Garcia, Angew. Chem. Int. Ed. 55 (2016) 5414–5445.
[3] Z.B. Fang, T.T. Liu, J. Liu, et al., J. Am. Chem. Soc. 142 (2020) 12515–12523.
[4] H.Q. Xu, J. Hu, D. Wang, et al., J. Am. Chem. Soc. 137 (2015) 13440–13443.
[5] S.C. Roy, O.K. Varghese, M. Paulose, C.A. Grimes, ACS Nano 4 (2010) 1259–1278.
[6] X. Chang, T. Wang, J. Gong, Energy Environ. Sci. 9 (2016) 2177–2196.
[7] Y. Lee, S. Kim, J.K. Kang, S.M. Cohen, Chem. Commun. 51 (2015) 5735–5738.
[8] H. Fei, M.D. Sampson, Y. Lee, C.P. Kubiak, S.M. Cohen, Inorg. Chem. 54 (2015) 6821–6828.
[9] K.G. Laurier, F. Vermoortele, R. Ameloot, et al., J. Am. Chem. Soc. 135 (2013) 14488–14491.
[10] B. An, Z. Li, Y. Song, et al., Nat. Catal. 2 (2019) 709–717.
[11] D. Wang, R. Huang, W. Liu, D. Sun, Z. Li, ACS Catal. 4 (2014) 4254–4260.
[12] G. Huang, Y. Wang, T. Liu, Chin. Chem. Lett. 30 (2019) 2309–2312.
[13] T. Li, B.-.T. Liu, Z.-.B. Fang, et al., J. Mater. Chem. A 9 (2021) 4687–4691.
[14] X.J. Hu, Z.X. Li, H. Xue, et al., CCS Chem. 2 (2020) 616–622.
[15] A.A. Zhang, X. Cheng, X. He, et al., Research 2021 (2021) 9874273.
[16] L. Li, J.D. Yi, Z.B. Fang, et al., Chem. Mater. 31 (2019) 7584–7589.
[17] B.T. Liu, X.H. Pan, D.Y. Nie, et al., Adv. Mater. 32 (2020) e2005912.
[18] X.F. Lu, P.Q. Liao, J.W. Wang, et al., J. Am. Chem. Soc. 138 (2016) 8336–8339.
[19] Z. Li, A.W. Peters, A.E. Platero-Prats, et al., J. Am. Chem. Soc. 139 (2017) 15251–15258.
[20] J.Y. Liang, W.N. Lipscomb, J. Am. Chem. Soc. 108 (1986) 5051–5058.
[21] C. Kormann, D.W. Bahnemann, M.R. Hoffmann, Environ. Sci. Technol. 22 (1988) 798–806.
[22] S. Merouani, O. Hamdaoui, F. Saoudi, M. Chiha, J. Hazard. Mater. 178 (2010) 1007–1014.
[23] Y.X. Ye, C. Wen, J. Pan, et al., Appl. Catal. B 285 (2021) 119726.
[24] Y. Xu, J. Mo, Q. Liu, X. Wang, S. Ding, Catal. Sci. Technol. 10 (2020) 2040–2046.
[25] G. Ye, P. Luo, Y. Zhao, et al., Chemosphere 253 (2020) 126767.
[26] Y.N. Gong, W. Zhong, Y. Li, et al., J. Am. Chem. Soc. 142 (2020) 16723–16731.
[27] C.A. Kent, J.J. Concepcion, C.J. Dares, et al., J. Am. Chem. Soc. 135 (2013) 8432–8435.
[28] D.-.C. Liu, H.J. Wang, T. Ouyang, et al., ACS Appl. Energy Mater. 1 (2018) 2452–2459.
[29] S.L. Chan, T.L. Lam, C. Yang, S.C. Yan, N.M. Cheng, Chem. Commun. 51 (2015) 7799–7801.
[30] Y. Liu, W. Wang, J. Electrochem. Soc. 159 (2012) D375–D381.